Express Polymer Letters Vol.18, No.11 (2024) 1077–1093
Available online at www.expresspolymlett.com
https://doi.org/10.3144/expresspolymlett.2024.83

Research article

Heat-sealable paper fabricated using a latex coating based on modified natural rubber filled with gelatin

Rattanawadee Ninjan[1], *Bencha Thongnuanchan*[1,2*], *Natinee Lopattananon*[1], *Subhan Salaeh*[1,2], *Phakawat Tongnuanchan*[3], *Pornsuwan Buangam*[4]

[1]Department of Rubber Technology and Polymer Science, Faculty of Science and Technology, Prince of Songkla University, 94000 Pattani, Thailand
[2]Research Unit of Advanced Elastomeric Materials and Innovations for BCG Economy (AEMI), Faculty of Science and Technology, Prince of Songkla University, 94000 Pattani, Thailand
[3]Department of Food Science and Nutrition, Faculty of Science and Technology, Prince of Songkla University, 94000 Pattani, Thailand
[4]Synchrotron Light Research Institute (Public Organization), 30000 Nakhon Ratchasima, Thailand

Received 14 June 2024; accepted in revised form 8 August 2024

Abstract. Research into sustainable packaging materials has gained increasing importance due to the pressing environmental concerns related to plastic waste. The present study focused on developing a sustainable paper coating based on modified natural rubber (NR) latex filled with gelatin (GT). The graft copolymer latex of NR and poly(vinylbenzyl chloride) bearing quaternary ammonium groups, abbreviated as NR-*g*-QPVBC, was first synthesized. GT was then incorporated into the latex, and the combination of these materials resulted in a heat-sealable film with good tensile properties and a water barrier. The ionic crosslinking of the latex film was achieved by the reaction with ethylenediaminetetraacetic acid (EDTA). Heat-sealing studies of the NR-*g*-QPVBC latex film filled with GT (NR-*g*-QPVBC/GT) revealed its heat-sealability at 160 °C. Scanning electron microscope (SEM) analysis further confirmed the diffusion of the chains across the interface during heat sealing. Dip coating was a method for depositing latex film on kraft paper. The paper coated with the NR-*g*-QPVBC/GT latex showed a significant increase in dry and wet-tensile strength compared to the uncoated paper. The sealing process was optimized to achieve a heat-seal strength of 755.31 N/m at a dwell time of 3 s and a temperature of 160 °C. The research's practical application was demonstrated by transforming the coated paper into various heat-sealable bags using a handheld bag sealer.

Keywords: *heat-sealable paper, natural rubber, graft copolymers, vinylbenzyl chloride*

---

1. Introduction

While the development of self-healing natural rubber (NR) has sparked significant interest, it is essential to acknowledge its challenges. Various methods have been utilized to transform NR into healable materials, often involving chemical modification of its structure [1]. The main healing mechanisms include reversible disulfide crosslinks [2, 3], hydrogen bonding [4, 5], ionic functional groups [6], and molecular interdiffusion/polar interactions [7–9], offering promising avenues for exploration. However, it is essential to note that these materials often demonstrate a mechanical performance inferior to traditional NR vulcanizates, highlighting the need for further research and innovation in this area.

Incorporating fillers into the NR and NR derivatives is a common way to improve mechanical properties. Additionally, incorporating functional or nanofillers in the rubber could generate novel healable materials. Hernández *et al.* [10] conducted a study to elucidate the influence of graphene loading (ranging from 0 to 2 phr) on the properties of self-healing NR.

---

[*]Corresponding author, e-mail: jjthongnuanchan@hotmail.com

The low reinforcement effect was observed with adding 0.5 phr graphene, attaining the highest tensile strength of 0.56 MPa and healing efficiency of about 53%. However, a noticeable increase in electrical conductivity of the nanocomposite was observed with the addition of graphene at 0.25 phr.

Le *et al*. [11] investigated the impact of carbon nanotube (CNT) on the self-healing ability of butyl imidazole-modified bromobutyl rubber (BIIR)/NR blends. The research revealed that the highest tensile strength (3.80 MPa) was achieved from a 10:90 blend ratio of NR:BIIR that contained 5 phr of CNT. The corresponding blend demonstrated a restored electrical conductivity after being healed at 120 °C for 10 min and subsequently at room temperature (*RT*) for 24 h. Cao *et al*. [12] utilized tunicate cellulose nanocrystals (t-CNs) as a nanofiller in the development of healable material from a modified NR, namely epoxidized natural rubber (ENR). The ability of t-CNs to participate in hydrogen bonding with oxygenous groups in the ENR molecule led to a significant improvement in its tensile properties and self-healing efficiency. The ENR exhibited a tensile strength of 4.04 MPa with the addition of 20 phr of t-CNs. Furthermore, a healing efficiency of 86% was observed for the corresponding nanocomposite after being healed at *RT* for 24 h.

Gelatin (GT) is a biomaterial obtained from the partial hydrolysis of collagen, which can be extracted from animals' bones, cartilage, and skin [13]. One of the most essential features of gelatin film is its heat-sealing capability, which enables it to be made into packaging. Many researchers have extensively investigated the heat-sealing properties of gelatin-based films [14, 15]. GT is composed predominantly of 18 complex amino acids, and the main functional groups in their structures are amide (–C=O–NH–), amino ($–NH_2$), carboxyl (–C=O–OH), and carboxylate groups ($–C=O–O^–$) [13]. Functional groups of gelatins play a vital role in the heat sealability of their films, particularly those that can form hydrogen bonding [15].

Our previous research [16] investigated developing thermally assisted healable films from graft copolymers of NR and poly(vinylbenzyl chloride) containing quaternary ammonium groups (NR-*g*-QPVBC). The heat treatment at 100 °C was a necessary step, stimulating interdiffusion across interfaces and providing a path for rubber chains to gradually undergo the reptation process at *RT* during the healing process. This study aimed to transform the NR-*g*-QPVBC into heat-sealing films by incorporating GT, a material known for its heat-sealable properties. The addition of GT into the graft copolymer latex was thought to combine the former's heat-sealable properties with the latter's exceptional tensile properties.

The practicality of the graft copolymer latex filled with GT was demonstrated by its use as a barrier coating for recycled kraft paper. Coating a heat-sealable layer on paper is a practical and efficient method for creating a secure seal. This is a significant practical benefit, often achieved with paper coated with synthetic polymers like polyethylene (PE), polypropylene (PP), or ethylene vinyl alcohol (EVOH) [17]. Adibi *et al*. [18] reported on utilizing NR latex as a barrier coating for paper, where alpha-1,3 glucan (9–50 wt%) was used as a functional additive to improve its mechanical strength and barrier properties. However, the ability of NR-based films to heat-seal has not been investigated and reported.

In the present system, the introduction of ionic crosslinking of NR-*g*-QPVBC was facilitated by the reaction with ethylenediaminetetraacetic acid (EDTA). The reversible ionic bonds were introduced to provide heat-seal strength for the graft copolymer film. EDTA could combine with polyvalent cations to form a complex due to the presence of its four carboxylate groups (Figure 1). Furthermore, many polymers bearing cationic groups (most commonly quaternary ammonium, QA) have been reported to have antimicrobial properties [19–21]. This led to the preliminary testing for the antibacterial activity of NR-*g*-QPVBC films using the disk diffusion method.

This innovative work was the first to report on developing a paper coating based on the NR-*g*-QPVBC latex filled with GT. The developed latex coating would provide a unique combination of good water repellency, wet strength, and heat-seal ability for a coated paper. Dip-coating paper with the NR-*g*-QPVBC/GT latex demonstrated the transformation of kraft paper into heat-sealable paper. The straightforward approach to producing a modified NR latex film with heat-sealing ability offers development opportunities in paper coating materials. The work also hints at the potential for further developing latex-coated paper into wet-strength papers. Using modified NR latex as barrier coatings on paper packaging also presents a promising and practical alternative to synthetic paper coatings. Therefore, the distinct advantages of this technique are its simplicity and

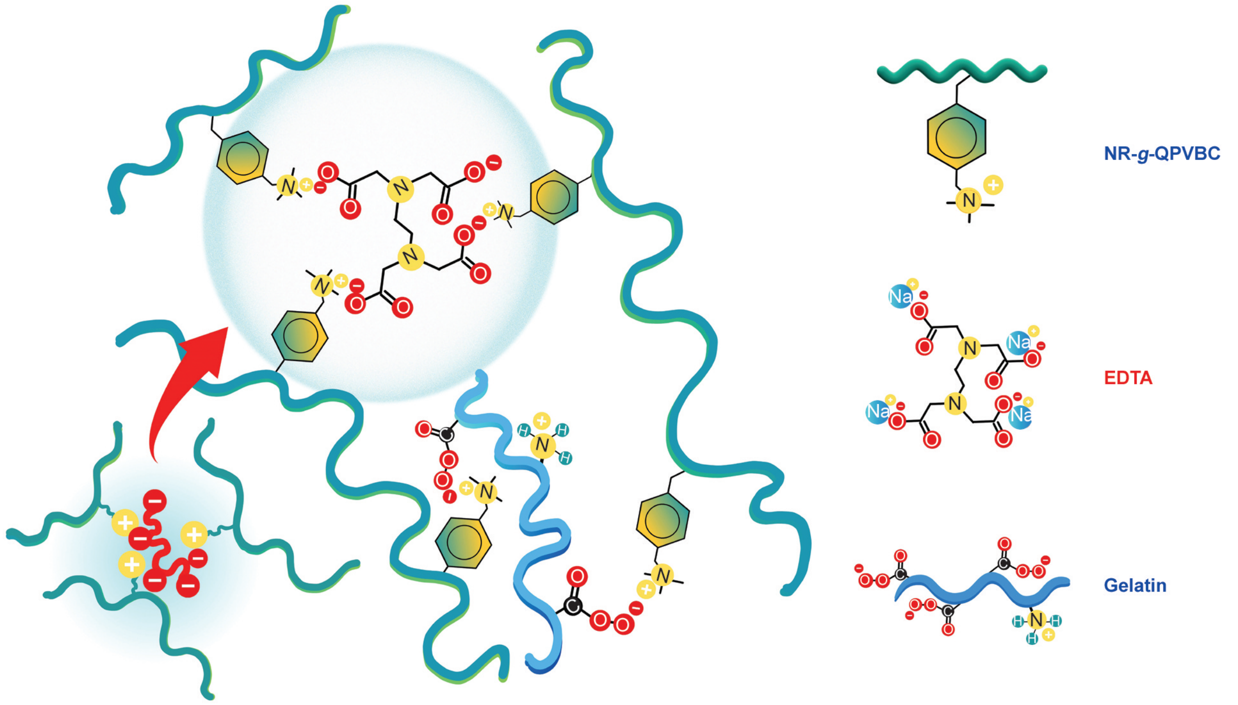

Figure 1. Proposed chemistry of ionic crosslinking and ionic interactions between cationic groups of NR-*g*-QPVBC with anions from tetrasodium ethylenediaminetetraacetic acid (EDTA) and GT, respectively.

sustainability. Moreover, the present paper also provided substantial results, demonstrating the potential of EDTA, typically used as a chelator for scavenging metal ions, in ionically curing the graft copolymer latex films.

2. Experimental

2.1. Materials

High ammonia concentrated natural rubber (HANR) was used to prepare graft copolymers latex. It contained a dry rubber content (DRC) of about 61 wt% and was manufactured by Yala Latex Co., Ltd. (Yala, Thailand). 4-Vinylbenzyl chloride (VBC) was purchased from Sigma-Aldrich Chemicals (Steinheim, Germany). A redox initiator couple of tetraethylenepentamine (TEPA) and *tert*-butyl hydroperoxide (*t*-BHP) was purchased from Fluka (Buchs, Switzerland). Sodium dodecyl sulfate (SDS) was used to stabilize the latex during the grafting reaction and was purchased from Sigma-Aldrich Chemicals (Steinheim, Germany). The gelatin was a type-B gelatin with a bloom strength ranging from ~220–240, extracted from bovine hide. It was supplied by Foodmate Co., Ltd. (Jiangxi, China). EDTA was manufactured by Merck KGaA (Darmstadt, Germany) and used as an anionic crosslinking agent. Recycled kraft paper with a base weight of ~110 g/m^2 was used to prepare heat-sealable papers. It was supplied by Plango Co., LTD (Bangkok, Thailand).

2.2. The preparation of NR-*g*-PVBC latex

The emulsion polymerization technique was employed to prepare the graft copolymers of NR-*g*-PVBC latex under a flowing nitrogen atmosphere at 50 °C. A 180 g of 2% ammonium hydroxide was first added to the reaction vessel containing NR latex (155 g) to adjust the total solids content to about 30%. The SDS (1 g) and TEPA (0.48 g) were then incorporated into the latex under stirring. Subsequently, a mixture of VBC (5 g) and *t*-BHP (0.48 g) was added dropwise into the reaction vessel. The resulting latex was stirred at *RT* for 3 h, allowing the monomer and *t*-BHP to partition into the latex particles. After the swelling period was completed, the reaction temperature was raised to 50 °C, and the reaction was allowed to proceed for 8 h at this temperature.

2.3. The preparation of the NR-*g*-QPVBC/GT latex

The quaternization of the NR-*g*-PVBC latex was carried out through the Menschutkin reaction [22] by reacting with trimethylamine (TMA). TMA (1.2 g, ~20 mmol) was first added into 80 g of latex (containing ~10 mmol of VBC) under continuous stirring.

The reaction was then carried out by heating the resulting latex to 50 °C and maintaining the temperature at this level for 3 h. The amount of TMA used for quaternization corresponded to a 2:1 molar ratio of TMA:VBC. Subsequently, three levels of GT (*i.e.*, 2, 4, 6 phr) were added to the latex, and the mixture was stirred continuously at 50 °C for 1 h. After being allowed to cool naturally, the resulting latex was stored at *RT* for further use.

2.4. Crosslinking of the NR-*g*-QPVBC/GT latex

An EDTA, a curing agent, was mixed into the NR-*g*-QPVBC/GT latex, and the mixture was stirred at *RT* for 10 min before being cast into a latex film. The added amount of EDTA was calculated based on the initial moles of VBC present in the grafting reaction, using a 0.5:1 molar ratio of EDTA:VBC. The latex film was then allowed to dry in a hot air oven at 60 °C until obtaining a constant weight. The tensile testing of the latex film was conducted at a crosshead speed of 500 mm/min according to the ASTM D412, using the Hounsfield Tensometer model H 10 KS (the Hounsfield Test Equipment Co., Ltd, Surrey, UK).

2.5. Morphological studies

Particle morphology of NR-*g*-PVBC latex was examined using a Talos F200i scanning/-transmission electron microscope (SEM/TEM). (Thermo Fisher Scientific, Waltham, USA). Phase contrast was enhanced by positively staining the NR phase with osmium tetroxide (OsO_4). The latex was diluted to about 0.05% total solids content using ammoniated water and then placed on a 400 mesh copper TEM grid. After air drying in a desiccator, the TEM gird was exposed to OsO_4 vapor for 1 h before viewing by TEM. An ultra-thin section of the latex film (~90 nm) was also prepared using RMC MT-XL ultra-microtomes (Boeckeler Instruments, Inc., Tucson, USA) at -150 °C for investigating film morphology. Contrast enhancement was also achieved by OsO_4 staining at *RT* for 1 h before TEM analysis.

2.6. X-ray photoelectron spectroscopy

The surface chemistry of the NR-*g*-QPVBC film was examined by X-ray photoelectron spectroscopy (XPS) using a Kratos AXIS Ultra DLD (Kratos Analytical, Manchester, UK). The film was analyzed using monochromatic Al-Kα radiation (1486.6 eV), operating at 150 W in hybrid mode with a pass energy of 20 eV at step sizes of 100 meV for high-resolution spectra. The XPS peak fitting was conducted using Kratos Vision 2 processing software.

2.7. Dynamic mechanical testing

Dynamic mechanical, thermal analysis (DMTA) was conducted under tension mode at a strain amplitude of 0.01% using a DMTA IV Dynamic Mechanic Thermo analysis instrument (Rheometric Scientific, Reichelsheim, Germany). The test frequency was 1.0 Hz, with a temperature of –80 to 200 °C and a 10 °C/min heating rate.

2.8. Equilibrium swelling measurement

The swelling test was performed to determine levels of crosslinking in latex films. First, a film was die-cut into a circular shape with a diameter of 20 mm, and its weight was determined to be the nearest 0.1 mg. The film was then immersed in toluene before being allowed to swell at *RT*. Once the film reached its equilibrium weight, it was dried to a constant weight. The de-swollen weight was then determined and recorded as *D*, and the amount of toluene absorbed in the film (A_s) was calculated. After that, the volume fraction of the rubber in the swollen film (V_r) was then determined by the Equation (1) [23]:

$$V_r = \frac{\frac{D-FT}{\rho_r}}{\frac{D-FT}{\rho_r} - \frac{A_s}{\rho_s}} \tag{1}$$

where *F* represents the volume fraction of the insoluble components (*i.e.*, SDS) in the film, and *T* is the initial weight of the film before swelling. ρ_r and ρ_s are the densities of rubber and solvent, respectively.

2.9. Wide-angle X-ray scattering (WAXS) analysis

WAXS was used to determine the degree of crystallinity in the NR-*g*-QPVBC films under strain. The measurement was carried out during the tensile deformation of the latex film, using in-situ stretching WAXS. The WAXS analysis was conducted using a Beamline 1.3 W at the Siam Photon Laboratory, Synchrotron Light Research Institute (SLRI), Nakhon Ratchasima, Thailand. The scattering pattern of the film was recorded using a CCD detector, Rayonix sx165 (Rayonix, L.L.C., Illinois, USA), with a diameter of 165 mm. The wavelength and the distance of the sample-to-detector were 0.138 and 115 mm, respectively. The film was first stretched with a constant crosshead speed of 50 mm/min to reach a given strain and then relaxed in the deformed state. The WAXS pattern was acquired at this state for 30 s before continuously stretching to the predetermined strain until the characterization was complete. The SAXS Image Tools (SAXSIT) program, developed by SLRI, was used to analyze WAXS data. The crystallinity (X_c) of the rubber was estimated from X-ray scattering results according to Equation (2) [24]:

$$X_c\,[\%] = \frac{A_c}{A_c + A_a} \cdot 100 \tag{2}$$

where A_c and A_a represent the area of the crystalline region and the area of the amorphous region, respectively.

2.10. Antimicrobial activity

The antibacterial activity of NR-*g*-QPVBC/GT film was evaluated using a disk diffusion test, as described by Yeddes *et al*. [25]. *Staphylococcus aureus* (*S. aureus* ATCC 23235) and *Escherichia coli* (*E. coli* 0157:H7 ATCC 35150) were used as test bacteria, representing gram-positive and gram-negative bacteria, respectively. The bacteria were obtained from the Department of Medical Sciences Ministry of Public Health, Nonthaburi, Thailand. A nutrient agar (GranuCult® Nutrient agar, Merch KGaA, Darmstadt, Germany) was prepared and used as a culture medium in this experiment. The sterile surface of agar was first swabbed with 0.1 mL of inoculums containing approximately $1 \cdot 10^8$ CFU/mL of *S. aureus* or *E. coli*. After that, the inoculated agar plate was incubated at 37 °C for 24 h before the diameter of the zone of inhibition was measured.

2.11. Contact angle measurement

Water contact angles on the surface of uncoated paper and paper coated with the NR-*g*-QPVBC/GT latex were measured by the sessile drop method at ambient humidity using a contact angle meter (DM300, Kyoma Interface Science Co., Saitama, Japan). The liquid drop profile was recorded using a microscope equipped with a CCD camera. The reported contact angle was the average value of at least 5 measurements at different film surface locations.

2.12. Heat-seal strength

The latex films were cut into two rectangular strips (25×20 mm) using a sample cutter. The thickness of the films was in the range of 1 and 1.5 mm. One strip was then placed on top of the other and heat-sealed at 160 °C with a sealing pressure of 2 bar (0.2 MPa) for different sealing times using a handheld impulse (S.N.MARK Ltd., Park, Nonthaburi, Thailand). The width of the seal area was about 2 mm. The seal strength of the sealed films was measured by a T-peeling test, following the standards set by the American Society for Testing and Materials ASTM F88-09. The peel test was performed at 25±2 °C at a 300 mm/min crosshead speed, using a Hounsfield Tensometer H 10 KS (Hounsfield Test Equipment Co., Ltd, Surrey, UK). After the peel test, the failure modes of the seal films were also examined visually.

2.13. Scanning electron microscopy (SEM)

An SEM (Quanta 400, Thermo Fisher Scientific, Erlangen, Germany) was employed to investigate the morphology of cross-section in the heat-sealing areas of latex films. Fracture surfaces were prepared by cold fracturing under liquid nitrogen prior to visualization by SEM.

2.14. Fourier-transform infrared spectroscopy (FTIR)

FTIR analysis was conducted to monitor changes in function groups present in the NR-*g*-QPVBC after a heat-sealing process. The spectra were acquired with a Fourier transform infrared (FTIR) spectrometer (Tensor 27 FTIR spectrometer, Bruker Optics, Ettlingen, Germany). The spectrometer was fitted with a diamond prism attenuated total reflectance (ATR) accessory. The measurement ranges from 4000 to 400 cm^{-1}, at a resolution of 4 cm^{-1}.

2.15. Cobb test

The Cobb test was used to evaluate the quantity of water absorbed by paper or coated paper, according to the TAPPI method T441. The paper specimen with a 12.5×12.5 cm dimension was prepared and weighed to the nearest 0.01 g. The cut specimen was then fastened inside the Cobb tester, having a cross-sectional area of 100 cm^2. After that, 100 cm^3 of water was poured into the test ring. The paper was allowed to be in contact with water for 60 s before the water was removed from the test ring. The remaining water on the surface was removed using blotting papers before its weight was measured. The weight difference before and after the test determined the Cobb's value, as Equation (3) [18]:

$$\text{Cobb value [g/m}^2\text{]} = \frac{m_2 - m_1}{\text{Area}} \quad (3)$$

where m_1 and m_2 are the weight of the paper specimen before and after the Cobb test, respectively.

3. Results and discussion

3.1. Preparation of NR-*g*-PVBC and NR-*g*-QPVBC

Vinylbenzyl chloride (VBC) was grafted onto NR molecules via emulsion polymerization using a redox initiator couple of TEPA and *t*-BHP. The *t*-butoxy radicals generated from this initiation system were expected to be primarily located at the particle/water interface. This crucially made the NR particle surface the primary locus of graft copolymerization (Figure 2a).

Since the C=C bonds in NR molecules had been positively stained with OsO_4 vapor, the NR phase appeared darker in the TEM image. Consequently, the brighter areas represented the grafted phase of poly(vinylbenzyl chloride) PVBC. As described in our previous work [16], the amount of grafted PVBC in the graft copolymers was estimated using proton nuclear magnetic resonance (^{1}H-NMR) analysis. Notably, the graft copolymers were observed to comprise approximately 3.58 wt% of PVBC at 89.20% conversion when prepared using 5 wt% of VBC.

The quaternization of the NR-*g*-PVBC latex was carried out by reacting with TMA to convert its chloromethyl groups into QA groups. The detailed procedure for the quaternization of grafted PVBC chains has been thoroughly described elsewhere [22]. Figure 2b shows the high-resolution XPS spectra of N 1s for NR-*g*-QPVBC, which could be deconvoluted into two components. The first peak at 400.00 eV was assigned to the nitrogen bound to carbon (N–C). The second peak at 401.4 eV was the correct binding energy for quaternary nitrogen ($-NR_3^+$). This observation is in line with the findings of earlier studies reported elsewhere [26–28]. It is worth mentioning that the NR-*g*-PVBC film before quaternization exhibited a single XPS peak at 400.3 eV. Thus, these results prove the successful quaternization of the NR-*g*-PVBC with TMA, yielding the quaternized NR-*g*-PVBC (NR-*g*-QPVBC), as depicted in Figure 1.

3.2. Ionic crosslinking

EDTA is a polyprotic acid with four carboxylate groups, which can deprotonate at a pH level of ≥8.0 [29]. When these groups deprotonate, they can combine with cations of QA groups in the NR-*g*-QPVBC, effectively acting as a crosslinking agent (Figure 1). This hypothesis was confirmed by the significant increase in the tensile strength of the NR-*g*-QPVBC

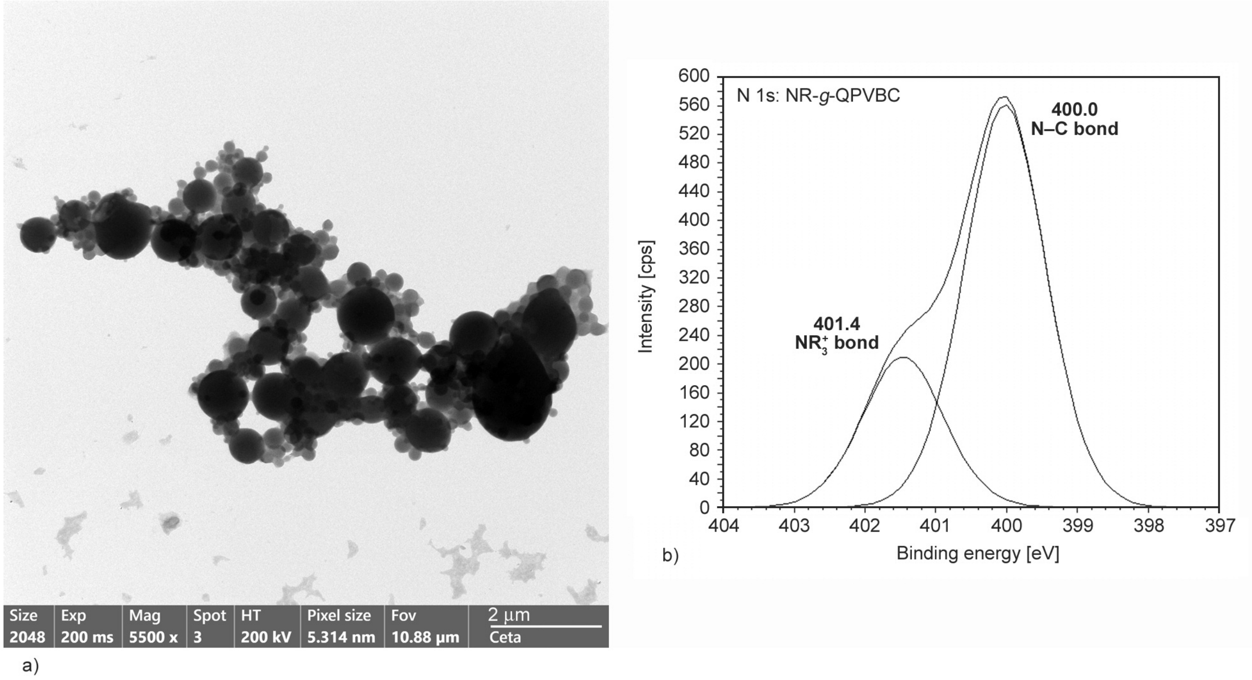

Figure 2. a) TEM micrograph revealing clusters of grafted poly(vinylbenzyl chloride) on the surface of NR particles and b) high-resolution XPS spectra of N 1s for NR-*g*-QPVBC.

film when EDTA was added (Figure 3a). The film's tensile strength increased from 7.72 to 14.10 MPa (an 82.64% increase), and it could withstand a strain of 1010%.

The effect of GT on the tensile strength of the NR-*g*-QPVBC film was then investigated. The latex films showed a significant increase in tensile strength with the addition of GT. The highest tensile strength was achieved by adding 4 phr of GT, abbreviated as NR-*g*-QPVBC/GT4 (Figure 3a). However, it is worth noting that increasing the GT loading beyond 6 phr led to the production of a cracked latex film during film formation. As a comparison, a pure gelatin film was found to have a tensile strength of approximately 36.46 MPa but a very low elongation at break (3.28%), as shown in the inserted graph in Figure 3a. Therefore, incorporating appropriate levels of GT into the NR-*g*-QPVBC film could significantly enhance its modulus and tensile strength, offering promising potential for future applications.

It is also anticipated that the carboxylate pendant groups (–C=O–O$^-$) along GT chains could ionically interact with the cationic QA groups of NR-*g*-QPVBC, potentially forming ionic crosslinks. This interaction has the potential to significantly improve the tensile strength of the NR-*g*-QPVBC films by incorporating GT. However, an increase in the concentration of GT from 4 to 6 phr did not significantly improve the film's tensile strength. This could be due to the limited number of cationic QA sites on the NR-*g*-QPVBC chains. These observations are consistent with the results obtained from determining the equilibrium volume fraction of rubber in the swollen state (V_r) of latex films. The values of V_r for the NR-*g*-QPVBC films filled with 0, 2, 4, and 6 phr of GT were 0.009, 0.105, 0.109, and 0.110, respectively. A higher value of V_r reflects a higher crosslink density in the latex film. In this experiment, the value of V_r was used to express the level of crosslinking in latex film due to the uncertainty in the value of the Flory-Huggins interaction parameter (χ). Details for determining the V_r value of latex films using the equilibrium swelling method in toluene are previously described elsewhere [23]. Thus, these results suggest that the optimum level of GT loading was 4 phr (NR-*g*-QPVBC/GT4), as it gave the optimal tensile properties of the latex film.

Ultra-thin sectioning of the cured NR-*g*-QPVBC/GT4 latex film was then prepared and subjected to OsO_4 vapor staining. The phase separation between the NR and grafted PVBC phases in the latex film became apparent due to the brighter appearance of the unstained PVBC phase (Figure 3b). This intriguing phenomenon is likely a result of the immiscibility between the two phases, which is influenced by their significant difference in solubility parameters. Specifically, the solubility parameter for NR is 17.0 MPa$^{1/2}$ [30], while that for PVBC is 20.3 MPa$^{1/2}$

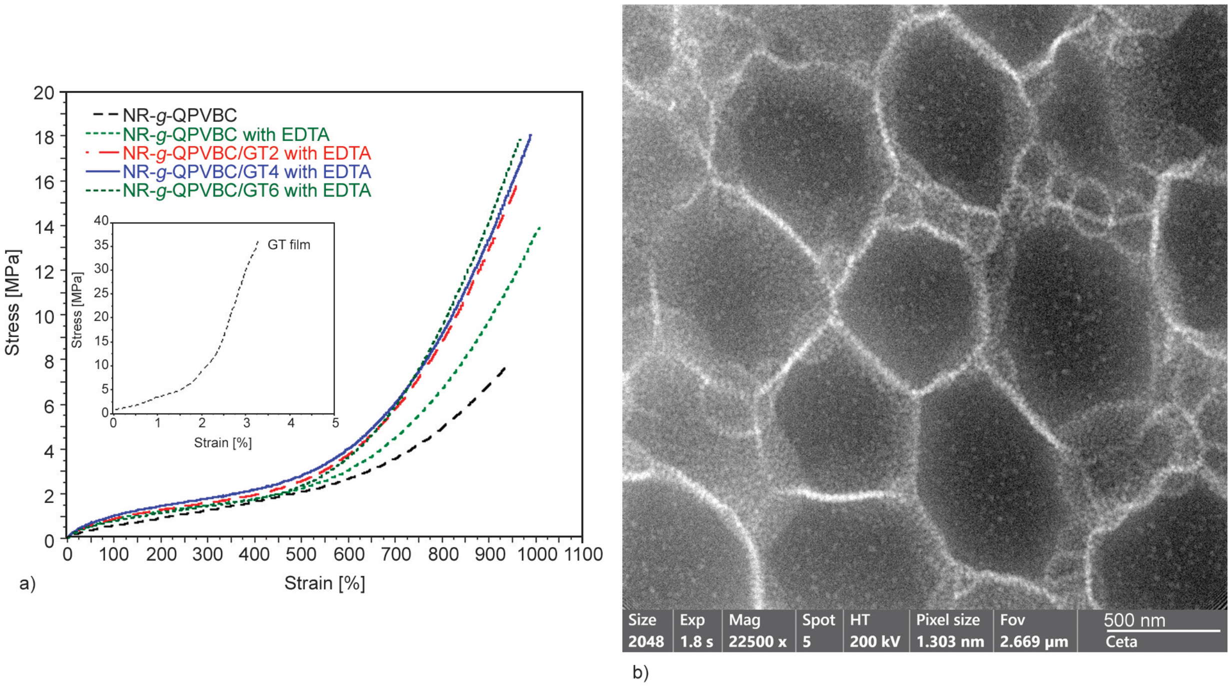

Figure 3. a) Stress-strain curves of uncured and cured NR-*g*-QPVBC films in the presence of different levels of GT (*i.e.*, 0, 2, 4, and 6 phr) and b) TEM micrograph for latex film cast from the NR-*g*-QPVBC/GT4 latex.

[31]. In addition, as the structure of GT does not contain active C=C double bonds, it cannot undergo an addition reaction with OsO_4. Thus, the GT phase would appear brighter than the NR phase and probably be located primarily at the particle boundaries. Consequently, the particle boundaries (the bright region) are expected to be predominantly composed of PVBC and GT phases. Figure 3b also reveals that the thickness of the bright regions ranged from 10–15 nm for the NR-*g*-QPVBC/GT4. At ambient temperatures, the boundaries between particles are expected to be rigid and immobilized. Thus, they could serve as physical crosslinks for the latex film as the molecules in the particle boundaries were chemically attached to the NR chains. As the temperature rises, the boundaries between rubber particles soften due to thermal energy disrupting ionic crosslinking in the NR-*g*-QPVBC/GT4. This allows chain segments to rearrange and slide over one another. This hypothesis was demonstrated by subjecting the NR-*g*-QPVBC/GT4 to DMTA analysis, providing an understanding of the material's behavior under varying temperatures.

Figure 4a illustrates the changes in the storage modulus (E') as a function of temperature for the uncured and cured NR-*g*-QPVBC films. As the temperature increased, a sharp drop of the E' was observed in the –71 to –66 °C range. It signified the beginning of the NR transition, indicating an increase in the mobility in either side chains or chain segments in its molecule. As the temperature continued to increase, the graft copolymer phase entered the glass transition region, leading to a drastic decrease in the E' by about three orders of magnitude.

In this experiment, the value of glass transition temperature (T_g) was determined from a temperature at which the loss tangent ($\tan\delta$) value reached a maximum. Figure 4b reveals that the T_g of the NR phases in the uncured films was about –59 °C. The T_g values of –56 and –54 °C were observed for the cured NR-*g*-QPVBC and NR-*g*-QPVBC/GT4 films, respectively. Moreover, the introduction of ionic crosslinking into latex films also reduced the magnitude of the $\tan\delta$ value for the NR phase. This suggests that the mobility of rubber chains became more restricted after ionic crosslinking was introduced into the NR-*g*-QPVBC film.

As the temperature was raised beyond this region, a second drop in the E' began to be observed at about –22 °C for all types of films. This corresponded to the transition of the NR-*g*-PVBC phase in the graft copolymers, giving a small $\tan\delta$ peak at about –19 °C. An increase in temperature above the T_g of the NR-*g*-PVBC phase led to a noticeable decrease in the E' for the uncured NR-*g*-QPVBC over a temperature range (*i.e.*, from –12 to 60 °C). It indicated the transition into a rubbery state before entering the flow region of the graft copolymers. The uncured NR-*g*-QPVBC exhibited a much more fluid-like behavior beyond this region, as its E' noticeably decreased with increasing temperatures.

The E' for the cured NR-*g*-QPVBC film tended to decrease gradually when heated, passing through the T_g region of the NR-*g*-PVBC phase. In contrast, the cured NR-*g*-QPVBC/GT4 exhibited a rubbery plateau region where a more-or-less constant E' was observed from about 60 to 160 °C. This suggests that the extent of ionic crosslinking formed in the

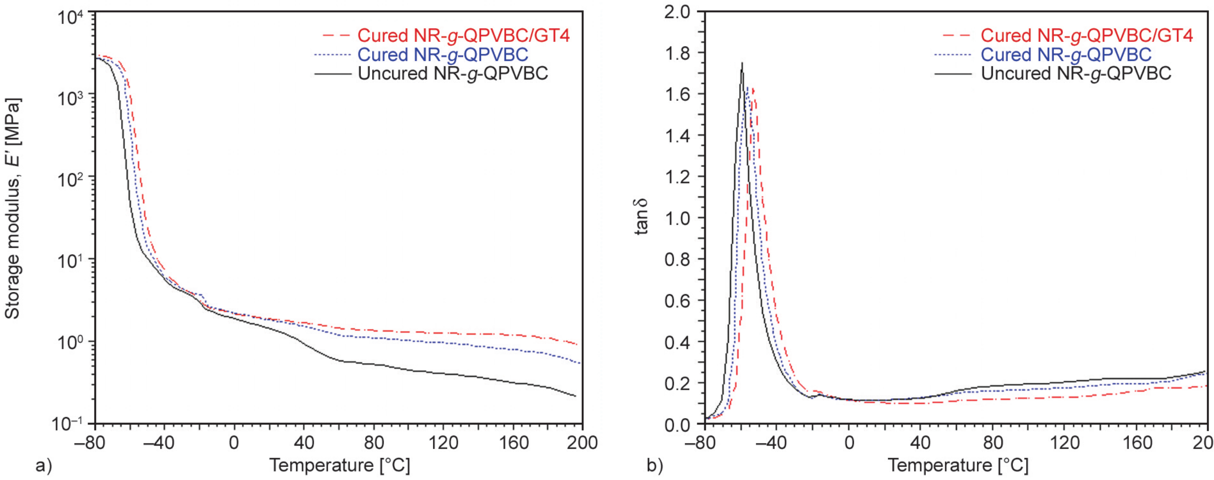

Figure 4. a) The storage modulus (E') and b) the loss tangent ($\tan\delta$) as a function of temperature for the uncured NR-*g*-QPVBC film and the cured NR-*g*-QPVBC and NR-*g*-QPVBC/GT4 films.

NR-*g*-QPVBC/GT4 film was greater than that of the cured NR-*g*-QPVBC film.

A noticeable decrease in the *E*′ of the NR-*g*-QPVBC/GT4 film was observed at about 178 °C, marking the onset of the terminal flow region. This means that ionic crosslinking in the NR-*g*-QPVBC/GT4 film is expected to be relatively stable up to about 178 °C. Beyond this temperature, ionic interactions are disrupted mainly by the applied thermal energy, allowing the rubber chains to move relative to one another. Therefore, the corresponding film is expected to display more fluid-like properties with further increasing temperature. These results provide a reliable basis for thermal stability and properties of the uncured and cured NR-*g*-QPVBC films in practical applications.

Additionally, it can also be seen from Figure 3a that the stress-strain curves for the cured NR-*g*-QPVBC/GT films differed from that of the cured film without GT. Hence, wide-angle X-ray scattering (WAXS) was conducted to monitor the films' strain-induced crystallization behaviors. The WAXS patterns obtained during the stretching of the cured NR-*g*-QPVBC films, with or without the addition of GT, at a 50 mm/min speed are shown in Figure 5a. The NR-*g*-QPVBC/GT4 was selected for further study in this experiment as it gave the optimum tensile properties.

Figure 5a provides clear evidence that, in both instances, the unstretched film displayed an amorphous halo ring, indicating a lack of preferred chain orientation. The emergence of crystalline diffraction spots signified the orientational behaviors of the rubber chains. Each diffraction spot corresponded to a specific crystallographic plane, providing evidence of the orientational behaviors of the rubber chains. Therefore, these results demonstrate the significant ability of the cured latex film to undergo strain-induced crystallization (SIC). However, the isotropic amorphous halo was still visible even at extensions of 490% strain. This suggests that only a small fraction of rubber chains underwent orientation along the stretching direction under the given experimental conditions.

The development of SIC in rubber films during stretching could be estimated from the WAXS intensity of the diffraction peaks produced by the (200) and (120) planes, as reported by Hernández *et al.*

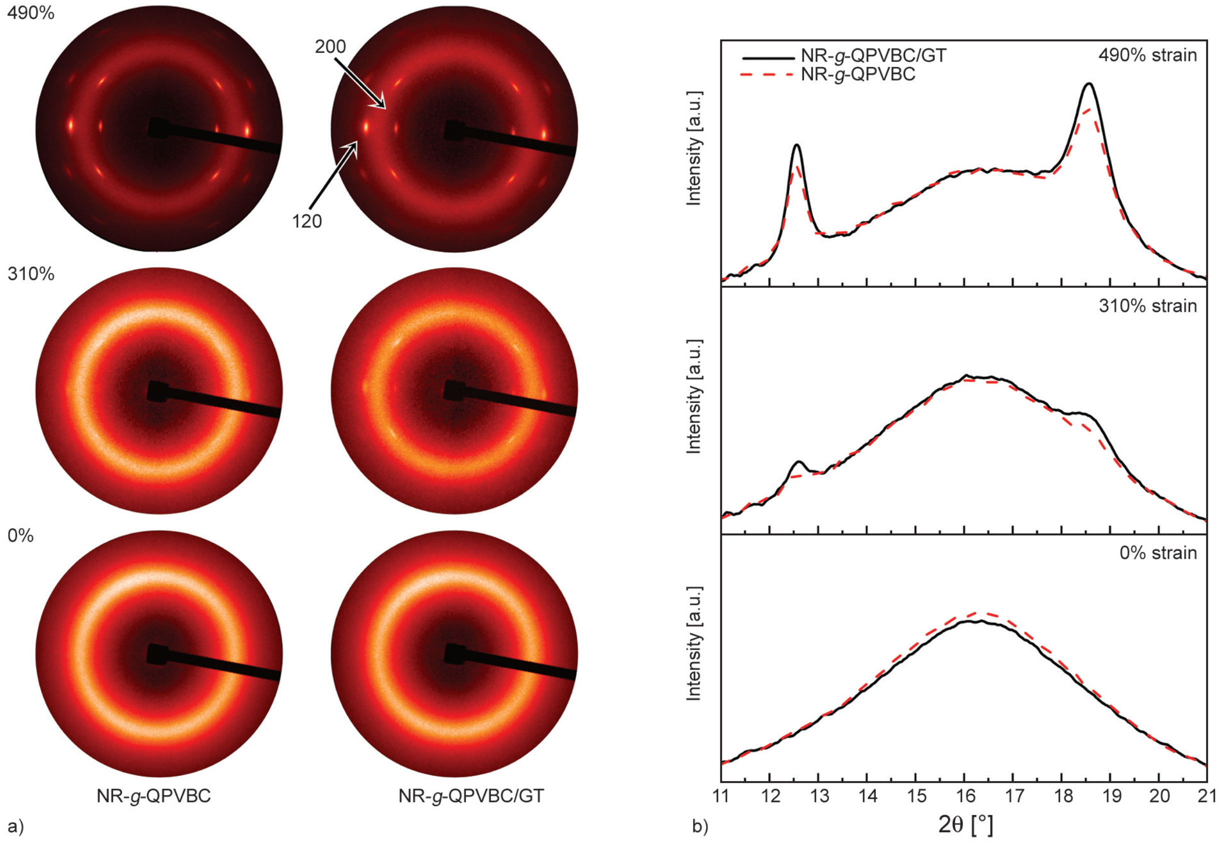

Figure 5. a) WAXS patterns of NR-*g*-QPVBC and NR-*g*-QPVBC/GT4 films upon stretching at 0, 310, and 490% strain at 25 °C, and b) WAXS intensity profiles *versus* 2θ for the corresponding films.

[24]. The diffraction peaks of the 200 and 120 planes occurred at 2θ of about 12.5° and 18.6°, respectively (Figure 5b). In all cases, WAXS patterns of the stretched films exhibited a peak centered at 2θ of ~ 16.4°, which corresponded to the amorphous phase of the rubber molecules with no preferred orientation of its chains. In contrast, the intensities of the two crystal diffraction peaks at 2θ of ~12.5° and 18.6° increased with strain during stretching, indicating the occurrence of SIC.

Furthermore, the mass fraction of the crystallinity index (X_c) in the stretched films could be estimated based on the area of a crystal diffraction peak relative to that of an amorphous halo peak, according to Equation (2). The X_c estimation indicated that the alignment of rubber chains in the stretching direction commenced at a strain of about 270% for both types of cured latex films (Figure 6a). As the strain increased, the X_c also showed a corresponding increase. However, the cured film with GT addition exhibited a higher degree of crystallinity, which became more evident at strains exceeding 300%. This finding suggests incorporating GT into the graft copolymer latex could promote rubber chain alignment during tensile deformation.

As the SIC of NR-*g*-QPVBC could be induced by the addition of GT, specific interactions between the two phases would be expected, leading to collaborative SIC (Figure 6b). GT is a polyampholyte that carries both positively and negatively charged groups [13]. A change in the charge distribution in GT's structure depends on the pH of the solution. At highly alkaline pH levels, the concentration of dissociated carboxyl groups (–C=O–O^-) increases, shifting the balance of charges towards the negative groups [33]. In this study, GT was introduced into a graft copolymer latex with a pH of approximately 10. This specific pH environment allowed the negatively charged groups of GT to interact ionically with the QA groups of the NR-*g*-QPVBC (Figure 1). The resulting ionic interaction would be expected to facilitate compatibility between the two phases.

3.3. Antimicrobial activity

Several polymers bearing cationic moieties have significant antimicrobial activity [19–21]. In diverse forms, QA cations are the most common cationic groups in these polymers, highlighting their potential in antimicrobial applications [34–36]. The cationic groups of these polymers can adsorb onto the negatively charged bacterial membrane through electrostatic interactions [20, 34]. The bactericidal activity of these polymers typically occurs by inducing membrane disruption by various mechanisms and ultimately causes the death of the bacteria.

As the NR-*g*-QPVBC/GT4 also contains QA cationic groups in its structure, its potential as an antimicrobial agent was assessed by examining the diameter of the zones of inhibition.

Figure 7 reveals that no inhibition zones against gram-negative *E. coli* and gram-positive *S. aureus* were observed for the cured NR-*g*-QPVBC/GT4 films. This lack of antibacterial activity suggests that the NR-*g*-QPVBC/GT4 film may not be suitable for applications where antibacterial properties are required. The films did not have antibacterial activity

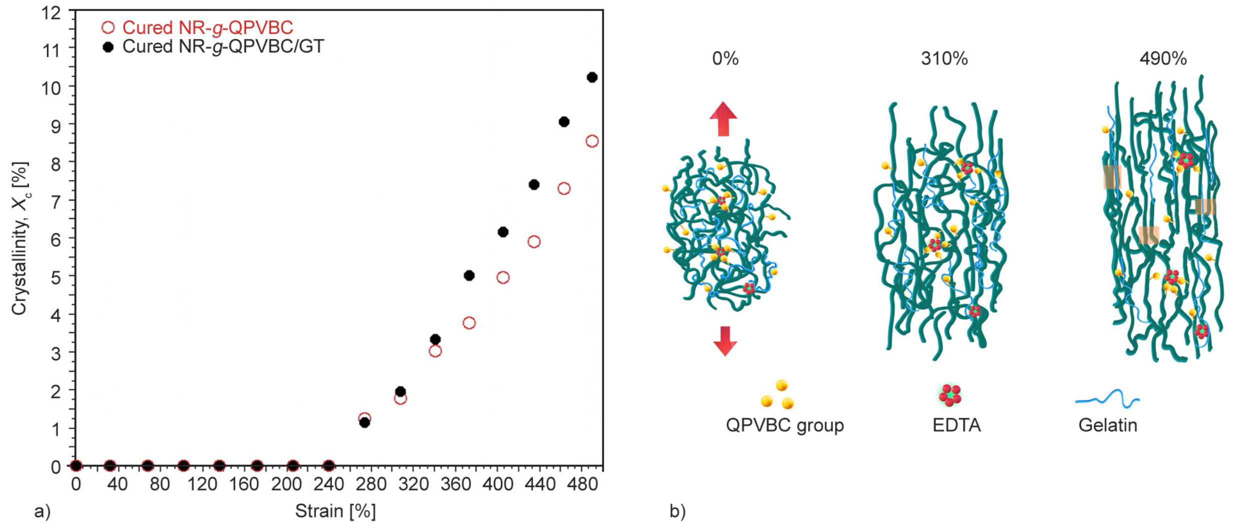

Figure 6. a) Crystallinity (X_c) as a function of strain for the cured NR-*g*-QPVBC and NR-*g*-QPVBC/GT4 films at 25 °C and b) crystallization model of the ionically crosslinked latex films, adapted from Tosaka *et al.* [32].

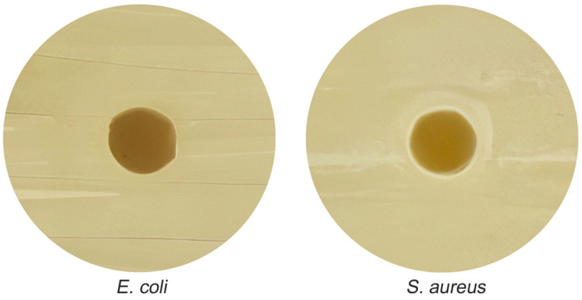
E. coli S. aureus

Figure 7. Images obtained from the disc diffusion test against *E. coli* and *S. aureus* for the cured NR-*g*-QPVBC/GT4 film.

against *E. coli and S. aureus* bacteria since they could not suppress their growth during an inhibition zone test. Although the NR-*g*-QPVBC molecules bear QA cationic groups, only a small amount (3.58 wt%) is present on its grafted chains. Thus, the possible explanation for this observation is that not enough QA cationic groups were present in the films to exhibit their antibacterial performance.

3.4. Heat-sealing ability

After that, the heat-seal ability of the NR-*g*-PVBC/GT4 films was thoroughly investigated, evaluating their promising potential as a heat-seal coating for papers. The sealing temperature is a critical parameter in the sealing process, ensuring chain interdiffusion occurs. This process is initiated by conducting the heat-sealing at a temperature above the T_g values of the main three phases in the film. The T_g values for the NR, NR-*g*-PVBC, and GT phases in the film were about –59, –19, and 63 °C, respectively.

Secondly, the applied thermal energy must be enough to break reversible ionic bonds in the film. Ionic interactions can ideally break and recombine under specific temperature ranges. This means that ionic moieties in the film can hop between ionic aggregates if enough thermal energy is applied. The ion-hopping weakens the ionic crosslinks and allows chain diffusion between sealing surfaces. A preliminary study revealed that the NR-*g*-QPVBC-based films were heat-sealable with an impulse heat-sealer of 160 °C.

It can be seen from Figure 8a that the NR-*g*-QPVBC/GT4 films exhibited a significantly higher seal strength than the NR-*g*-QPVBC film. During impulse sealing, two films were pressed together between a heated metal wire to promote the diffusion of polymer chains across the sealing interface. Thus, another major factor affecting the seal strength is the dwell time. It is a contact time in which the two surfaces are pressed together to create good contact over the sealing area (inserted image in Figure 8a). A suitable dwell time generally results in a strong seal since it promotes the formation of chain entanglement during the health-sealing process. The results suggest that the minimum dwell time for the NR-*g*-QPVBC/GT4 film with thickness ranging

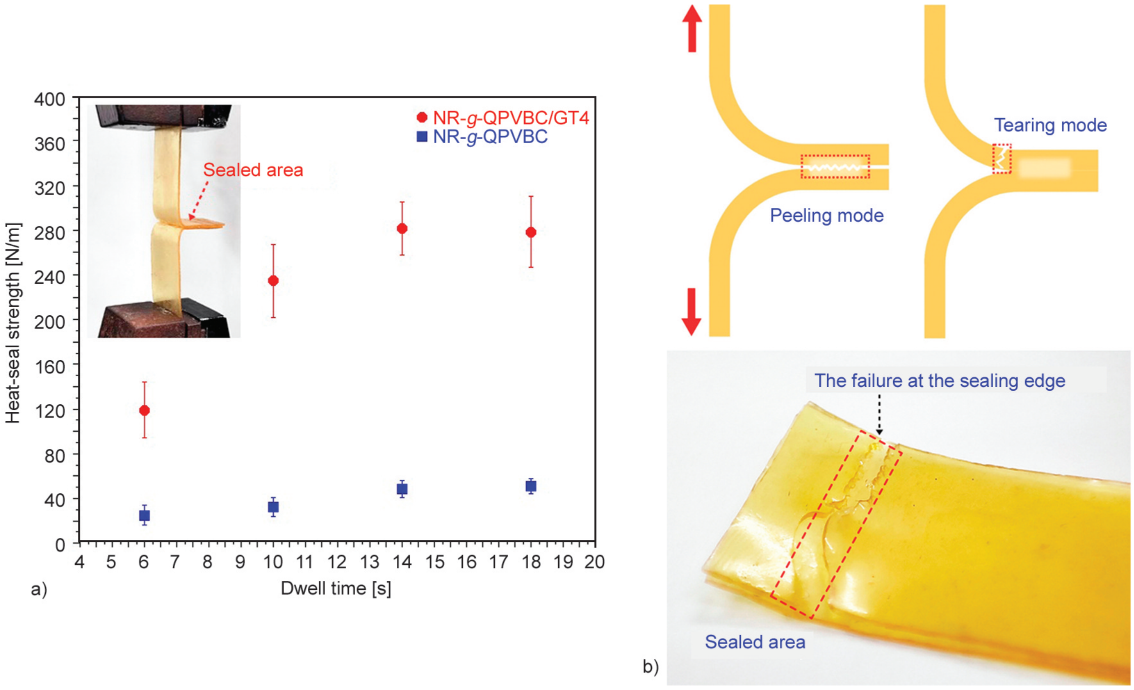

Figure 8. a) The heat-seal strength of the cured NR-*g*-QPVBC and NR-*g*-QPVBC/GT4 films at different dwell times, and b) failure modes of the sealed latex films and the failed specimen.

from ~1 to 1.5 mm at 160 °C was 14 s, as it gave the highest seal strength when using a sealing pressure of ~0.2 MPa. This finding is significant as it provides practical insights into optimizing the sealing process for NR-*g*-QPVBC-based films filled with GT.

Additionally, the average molecular weight of polymers is a crucial factor in determining the chain diffusion rate. This is particularly significant as it directly influences the movement of polymer chains during healing, a process known as reptation [37], where the chains move like a snake, sliding past each other. Hence, the rate of chain movement is crucial for the film's heat-seal ability, which is inversely related to the molecular weight. The average molecular weight of GT with a high bloom number (225) ranges from $5\cdot10^4$ to $10\cdot10^4$ g/mol, much lower than that of the graft copolymers. This implies that the GT chains are expected to travel across the sealing interface more quickly and at a longer distance than high-molecular-weight rubber chains during heat-sealing (Figure 9). The higher heat-seal strength observed for the NR-*g*-PVBC/GT4 films further confirms the role of chain entanglements across the healing interface.

In this study, the seal failure mode was scrutinized by visually examining the failed specimens. Three distinct failure modes are typically identified for measuring seal strength in a peel test: peeling, tearing, and a combination of both. Each of these modes offers valuable insights into the extent of interfacial diffusion and, consequently, the seal quality. The observed failure mode for the NR-*g*-QPVBC films was the peeling failure, which occurred when the interface between the bonded films separated during a peel test. This debonding of the film interface indicated a relatively low extent of interfacial diffusion over the sealed zone (Figure 8b).

When 4 phr of GT was introduced into the film, tearing failure was attained. This type of failure occurs when polymer chains from two opposite surfaces diffuse across the interfacial zone, leading to molecular entanglement. Interestingly, it was found that the tearing failure tended to occur at the seal edge (Figure 8b). It indicates that the energy required to cause seal separation during a peel test also included energy to deform test pieces. Therefore, the occurrence of tearing failure suggests that the sealing interface between the films is more robust than their bulk properties.

The findings reveal that the incorporation of GT into the NR-*g*-QPVBC film plays a pivotal role in promoting the extent of molecular diffusion across the sealing interface, leading to the creation of chain entanglements. This is clearly reflected in the increase in the seal strength of the interface and the subsequent change in the failure mode to tearing failure. It underscores the significant impact of GT on seal strength and molecular diffusion in NR-*g*-QPVBC films.

SEM analysis was used to demonstrate molecular diffusion along the sealed area. The sealed films were first cross-sectioned using freeze fracturing before their morphology was examined. A complete fusion along the sealing interface was observed for the NR-*g*-QPVBC/GT4 since the welding line between the two surfaces could not be identified (Figure 10). The result suggests that the NR-*g*-PVBC/GT4 film could merge during heat sealing, allowing molecular entanglement to form and providing good seal strength.

The FTIR spectra of the NR-*g*-QPVBC/GT4 film before and after heat-sealing at 160 °C for 14 s were also analyzed for changes in its functional groups, as illustrated in Figure 11. The absorption peaks at 2964 and 837 cm^{-1} were assigned to the $–CH_2–$ stretching and =C–H out-of-plane bending of the *cis*-1,4-polyisoprene, respectively [38]. The peak at 1240 cm^{-1} corresponded to the C–N stretching of

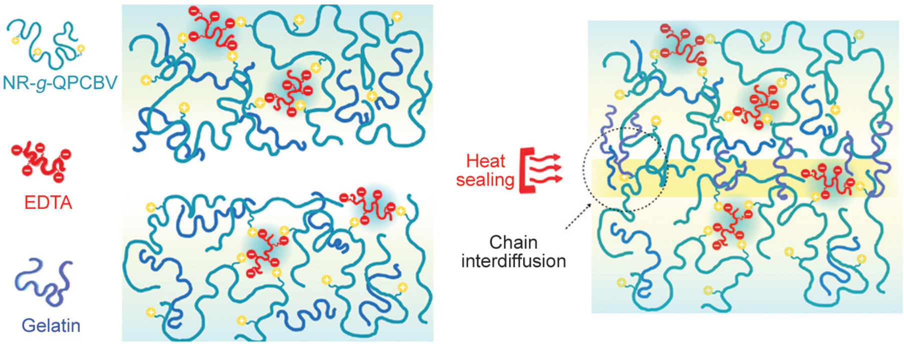

Figure 9. Interdiffusion of GT and NR-*g*-QPVBC chains occurred in the heat-seal area of the NR-*g*-QPVBC/GT4 film.

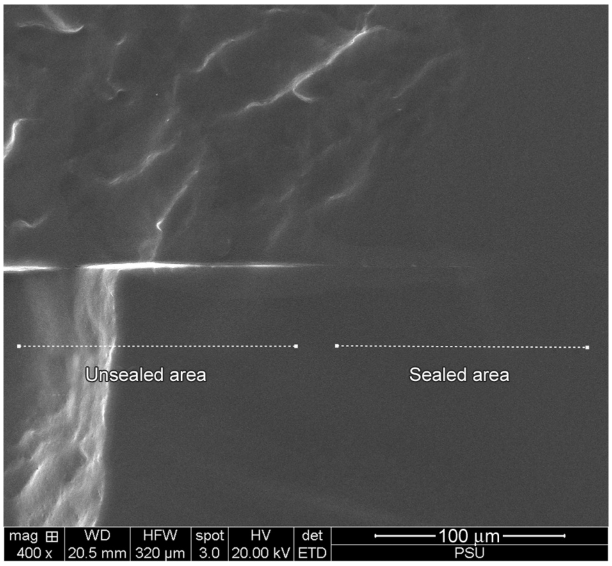

Figure 10. SEM micrographs of the cross-section at the sealing edge of the NR-*g*-QPVBC/GT4 film after being sealed at 160 °C for 14 s.

aliphatic amine in the quaternized PVBC (QPVBC) of the grafted chains.

Generally, the stretching vibration of C=C bonds in the NR molecules appears at about 1660 cm^{-1}. Unfortunately, the corresponding peak occurred close to the absorption of C=O stretching in amide groups present in GT. The characteristic bands typically found in the FTIR spectra of GT can be denoted as amide-I (1600–1700 cm^{-1}) and amide-II (1570–1520 cm^{-1}) [39]. The amide-I band is mainly associated with the absorptions corresponding to the C=O stretching of amide groups in GT molecules. Hence, the peak at 1656 cm^{-1} in the spectra of the NR-*g*-QPVBC/GT4 film could result from the absorptions of both the C= C stretching of NR coupled with the C=O stretching of GT.

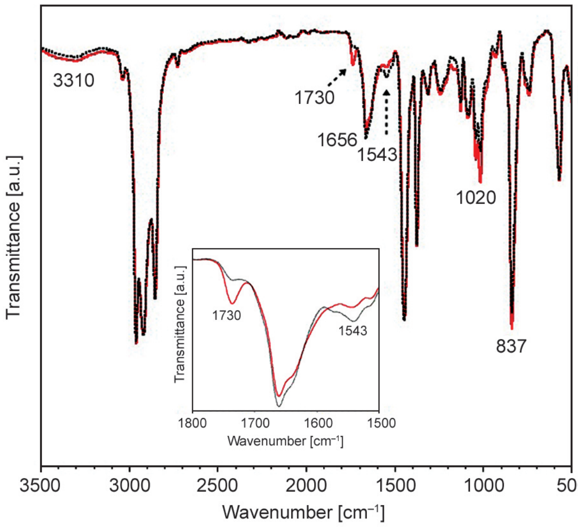

Figure 11. An overlay of FTIR spectra for the NR-*g*-QPVBC/GT4 film before and after heat-sealing at 160 °C for 14 s.

The amide-II band results from the N–H bending vibration with a minor contribution from the C–N stretching vibration. The inserted image in Figure 11 revealed a decrease in the intensity of the amide-II peak after the NR-*g*-QPVBC/GT4 film was heat-sealed at 160 °C for 14 s. Sufficient thermal energy is required to overcome forces of attraction between the polymer chains (*i.e.*, most importantly, ionic and hydrogen bonds) during a heat-sealing process, allowing the chain's diffusion across the sealing interface. H-bonding interactions between amide groups of GT occur primarily through the C=O and N–H functional groups. However, it has been reported that the N–H vibration modes are susceptible to their ability to form H-bonding [40]. In general, the FTIR peak intensity depends on the number of bonds related to the absorption, and an absorption band with fewer bonds involved exhibits a lower intensity. Thus, a reduction in the intensity of the amide-II band suggests that fewer N–H bonds were involved in forming H-bonding after a heat-sealing process. Tongnuanchan *et al.* [41] reported a similar observation after the films based on fish skin gelatin were heat-sealed at 150 °C for 1 s.

Furthermore, a significant increase in the intensity of the absorption peak at 1730 cm^{-1} was also observed after the film was heat-sealed. This suggests the occurrence of thermal oxidative degradation of GT during a heat-sealing process at 160 °C, which could result in the formation of degradation products containing carbonyl groups, –C=O (*e.g.*, aldehyde, ketone, ester, and carboxylic acid) [41].

3.5. Water absorptivity and tensile strength of coated paper

The NR-*g*-QPVBC/GT4-coated paper was prepared using the dip coating method. This involved immersing the paper in compounded latex to deposit the rubber coating. After the aqueous phase was removed through evaporation, a dry coating film of NR-*g*-QPVBC/GT4 was formed on the paper surface. The Cobb 60 test, a standard method for measuring the water absorptivity of paper, was then conducted. This test measures the quantity of water absorbed by a paper in 60 s. A high Cobb 60 value indicates high water absorption, which in turn suggests poor water repellency.

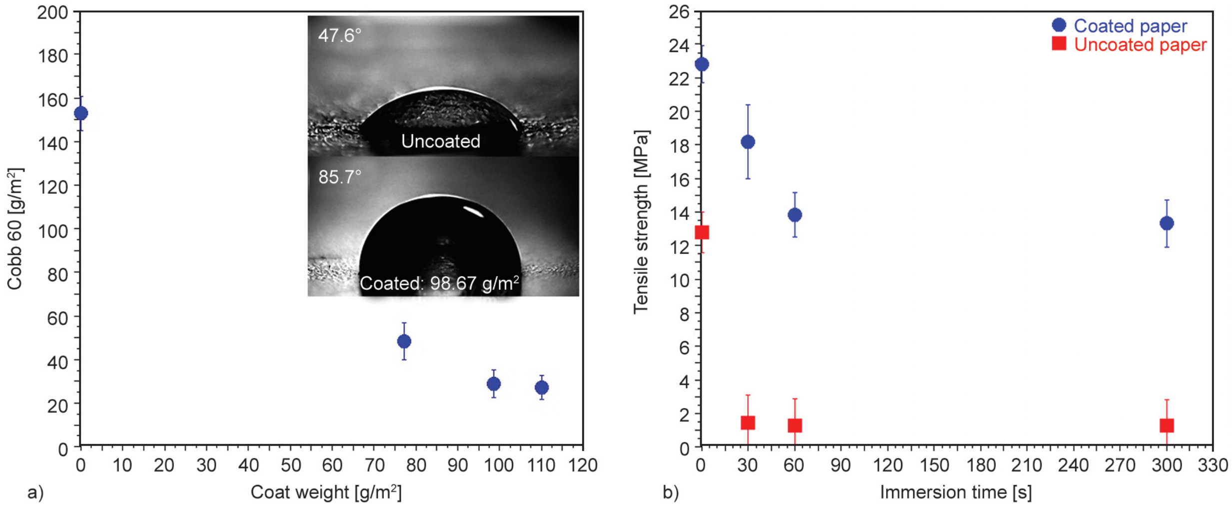

Figure 12. a) Cobb 60 values for the uncoated paper and paper coated with the NR-*g*-QPVBC/GT4 latex using different coat weights, and b) the wet tensile strength of the uncoated and coated paper with a coat weight of 98.6 g/m^2.

Figure 12a shows that the uncoated paper had a Cobb 60 value of 152.9 g/m^2, indicating poor water barrier performance. The Cobb 60 value significantly decreased to 48.3 g/m^2 when the paper was single-dipped into the NR-*g*-QPVBC/GT4 latex, demonstrating a remarkable improvement in water absorptivity. This was achieved with a coating thickness of 37 µm and a coat weight of 77.3 g/m^2. The coating thickness and coat weight required for achieving the optimum value of Cobb 60 (28.9 g/m^2) were 45 µm and 98.6 g/m^2, respectively, which was prepared using a double-dip process.

Changes in the wettability of a water droplet on the paper surface were also observed after being coated with the NR-*g*-QPVBC/GT4 latex. A water droplet initially made a contact angle of 47.6±6° with a paper surface (inserted images in Figure 12a). However, the water contact angle dramatically increased to 85.7±4° when the paper was coated with the latex using the optimum coat weight. This wettability alteration toward the non-wetting of the paper surface is mainly due to the hydrophobic nature of the latex coating. Generally, a higher hydrophobicity indicates better water barrier properties, which are essential for packaging applications.

Additionally, the application of a latex coating layer on the paper surface proved to be a significant factor in enhancing the tensile strength. Figure 12b clearly demonstrates that the coated paper exhibited a notably higher tensile strength than the uncoated paper. Moreover, the wet strength of the paper showed a substantial increase after it was coated with latex coating. A 90.2% decrease in tensile strength was observed after the uncoated paper was immersed in distilled water for 60 s, according to ASTM D829-97. This reduction is primarily due to water's disruption of hydrogen bonding in paper. However, the coated paper managed to retain 60.8% of its dry-tensile strength, giving a wet-tensile strength of 13.8 MPa. The higher wet-tensile strength indicates that the coated paper exhibits significantly lower water sensitivity than the uncoated paper.

3.6. Heat-seal strength of coated paper

In this system, the heat-seal characteristic of the coated paper relied on the latex coating's ability to adhere to itself after being heated under slight pressure. This is because the two layers of uncoated paper could not be sealed to each other by applying heat and pressure. The heat-sealing was conducted using a handheld bag sealer at 160 °C and varied dwell times, producing a 3 cm width of the seal area. The sealing time of 3 s was observed to be the optimum dwell time as it gave the highest heat-seal strength for the coated film, with the coating thickness ranging from 35–45 µm (Figure 13a). The failure mode of the heat-sealed paper was then examined after it was separated into two pieces. It can be seen from an inserted image in Figure 13a that two pieces of coated paper did not separate at the interface, and the sealing area remained intact. Therefore, the failure was not interfacial but within the bulk paper, leaving paper layers on both surfaces. The substrate failure indicated good seal strength as the paper failed before the sealing area of the coating material.

Heat-sealable paper has a significant environmental advantage and can be used in various applications.

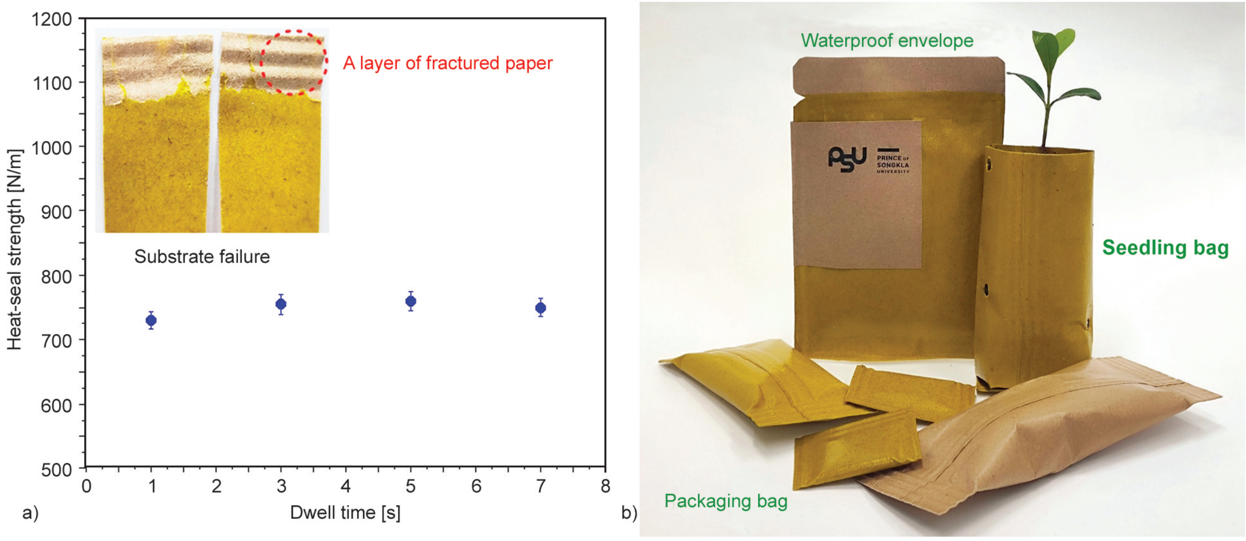

Figure 13. a) Heat-seal strength of paper coated with the NR-*g*-QPVBC/GT4 latex with different dwell times and b) the different types of heat-sealable bags made using the latex-coated paper.

It can be manufactured into custom-size waterproof envelopes and bags, offering a sustainable alternative to plastic packaging. The coated paper could be shaped into a seedling bag using a handheld sealer, as shown in Figure 13b. Using it as an alternative material for plastic seedling bags demonstrates its versatility and contributes to reducing plastic packaging waste.

4. Conclusions

This study demonstrated the potential of NR-*g*-QPVBC/GT latex as a paper-coating material with practical applications in sustainable packaging. The crosslinking in this system was achieved by using EDTA as a crosslinker, creating ionic interactions between polymer chains. Tensile testing and DMTA analysis provided irrefutable evidence that ionic crosslinking occurred in the NR-*g*-QPVBC latex film in the presence of EDTA. The heat-seal ability of the latex films was first examined to evaluate the promising potential of heat-seal coatings for papers. The result revealed that the NR-*g*-QPVBC latex films, with or without GT, were heat-sealable at 160 °C. However, incorporating GT into the graft copolymer latex resulted in a significantly higher seal strength than the film without GT. The latex film filled with GT was deposited on recycled kraft paper using a dip coating method. A significant reduction of the Cobb 60 value from 152.9 to 28.9 g/m^2 indicated a considerable decrease in the paper's water absorptivity after being coated with a coat weight of 98.6 g/m^2. The coated paper could also retain about 60.8% of its dry-tensile strength when immersed in water for 60 s. The dwell time required to produce the optimum heat-seal strength for the paper coated with the NR-*g*-QPVBC/GT4 was 3 s at 160 °C. The practicality of the heat-sealable paper was demonstrated by transforming it into different types of bags by folding and sealing the edges using a handheld bag sealer.

Acknowledgements

This research was supported by the National Science, Research, and Innovation Fund (NSRF) and Prince of Songkla University for the Fundamental Funds through grant No. SAT6601168c. Prince of Songkla University also supported this work under the Postdoctoral Fellowship Program.

References

[1] Santana M. H., den Brabander M., García S., van der Zwaag S.: Routes to make natural rubber heal: A review. Polymer Reviews, **58**, 1–25 (2018).
https://doi.org/10.1080/15583724.2018.1454947

[2] Hernández M., Grande A. M., van der Zwaag S., Garcia S. J.: Monitoring network and interfacial healing processes by broadband dielectric spectroscopy: A case study on natural rubber. ACS Applied Materials and Interfaces, **8**, 10647–10656 (2016).
https://doi.org/10.1021/acsami.6b02259

[3] Hernández M., Grande A. M., Dierkes W., Bijleveld J., van der Zwaag S., García S. J.: Turning vulcanized natural rubber into a self-healing polymer: Effect of the disulfide/polysulfide ratio. ACS Sustainable Chemistry and Engineering, **4**, 5776–5784 (2016).
https://doi.org/10.1021/acssuschemeng.6b01760

[4] Chino K., Ashiura M.: Themoreversible cross-linking rubber using supramolecular hydrogen-bonding networks. Macromolecules, **34**, 9201–9204 (2001).
https://doi.org/10.1021/ma011253v

[5] Liu J., Wang S., Tang Z. H., Huang J., Guo B. C., Huang G. S.: Bioinspired engineering of two different types of sacrificial bonds into chemically cross-linked cis-1,4-polyisoprene toward a high-performance elastomer. Macromolecules, **49**, 8593–8604 (2016).
https://doi.org/10.1021/acs.macromol.6b01576

[6] Xu C., Cao L., Lin B., Liang X., Chen Y.: Design of self-healing supramolecular rubbers by introducing ionic cross-links into natural rubber *via* a controlled vulcanization. ACS Applied Materials and Interfaces, **8**, 17728–17737 (2016).
https://doi.org/10.1021/acsami.6b05941

[7] Rahman M. A., Penco M., Peroni I., Ramorino G., Grande A. M., Di Landro L.: Self-repairing systems based on ionomers and epoxidized natural rubber blends. ACS Applied Materials and Interfaces, **3**, 4865–4874 (2011).
https://doi.org/10.1021/am201417h

[8] Rahman M. A., Penco M., Peroni I., Ramorino G., Janszen G., Di Landro L.: Autonomous healing materials based on epoxidized natural rubber and ethylene methacrylic acid ionomers. Smart Materials and Structures, **21**, 035014 (2012).
https://doi.org/10.1088/0964-1726/21/3/035014

[9] Rahman M. A., Sartore L., Bignotti F., Di Landro L.: Autonomic self-healing in epoxidized natural rubber. ACS Applied Materials and Interfaces, **5**, 1494–1502 (2013).
https://doi.org/10.1021/am303015e

[10] Hernández M., Bernal M. M., Grande A. M., Zhong N., van der Zwaag S., García S. J.: Effect of graphene content on the restoration of mechanical, electrical and thermal functionalities of a self-healing natural rubber. Smart Materials and Structures, **26**, 085010 (2017).
https://doi.org/10.1088/1361-665X/aa71f5

[11] Le H. H., Hait S., Das A., Wießner S., Stöckelhuber K. W., Böhme F., Reuter U., Naskar K., Heinrich G., Radusch H-J.: Self-healing properties of carbon nanotube filled natural rubber/bromobutyl rubber blends. Express Polymer Letters, **11**, 230–242 (2017).
https://doi.org/10.3144/expresspolymlett.2017.24

[12] Cao L., Yuan D., Chen Y., Xu C.: Biobased, self-healable, high strength rubber with tunicate cellulose nanocrystals. Nanoscale, **9**, 15696–15706 (2017).
https://doi.org/10.1039/C7NR05011A

[13] Alipal J., Mohd Pu'ad N. A. S., Lee T. C., Nayan N. H. M., Sahari N., Basri H., Idris M. I., Abdullah H. Z.: A review of gelatin: Properties, sources, process, applications, and commercialisation. Materials Today: Proceedings, **42**, 240–250 (2021).
https://doi.org/10.1016/j.matpr.2020.12.922

[14] Liu C., Huang J., Zheng X., Liu S., Lu K., Tang K., Liu J.: Heat sealable soluble soybean polysaccharide/gelatin blend edible films for food packaging applications. Food Packaging and Shelf Life, **24**, 100485 (2020).
https://doi.org/10.1016/j.fpsl.2020.100485

[15] Ciannamea E. M., Castillo L. A., Barbosa S. E., de Angelis M. G.: Barrier properties and mechanical strength of bio-renewable, heat-sealable films based on gelatin, glycerol and soybean oil for sustainable food packaging. Reactive and Functional Polymers, **125**, 29–36 (2018).
https://doi.org/10.1016/j.reactfunctpolym.2018.02.001

[16] Ninjan R., Thongnuanchan B., Lopattananon N., Salaeh S., Thitithammawong A.: Thermally assisted healable film based on modified natural rubber-bearing benzyl chloride functionality. Express Polymer Letters, **18**, 742–759 (2024).
https://doi.org/10.3144/expresspolymlett.2024.55

[17] Mujtaba M., Lipponen J., Ojanen M., Puttonen S., Vaittinen H.: Trends and challenges in the development of bio-based barrier coating materials for paper/cardboard food packaging; A review. Science of the Total Environment, **851**, 158328 (2022).
https://doi.org/10.1016/j.scitotenv.2022.158328

[18] Adibi A., Valdesueiro D., Mok J., Behabtu N., Lenges C., Simon L., Mekonnen T. H.: Sustainable barrier paper coating based on alpha-1,3 glucan and natural rubber latex. Carbohydrate Polymers, **282**, 119121 (2022).
https://doi.org/10.1016/j.carbpol.2022.119121

[19] Namivandi-Zangeneh R., Wong E. H. H., Boyer C.: Synthetic antimicrobial polymers in combination therapy: Tackling antibiotic resistance. ACS Infectious Diseases, **7**, 215–253 (2021).
https://doi.org/10.1021/acsinfecdis.0c00635

[20] Yang Y., Cai Z., Huang Z., Tang X., Zhang X.: Antimicrobial cationic polymers: From structural design to functional control. Polymer Journal, **50**, 33–44 (2018).
https://doi.org/10.1038/pj.2017.72

[21] Konai M. M., Bhattacharjee B., Ghosh S., Haldar J.: Recent progress in polymer research to tackle infections and antimicrobial resistance. Biomacromolecules, **19**, 1888–1917 (2018).
https://doi.org/10.1021/acs.biomac.8b00458

[22] van Ravensteijn B. G. P., Kegel W. K.: Colloids with continuously tunable surface charge. Langmuir, **30**, 10590–10599 (2014).
https://doi.org/10.1021/la501993c

[23] Ellis B., Welding G. N.: Estimation, from swelling, of the structural contribution of chemical reactions to the vulcanization of natural rubber. Part I. General method. Rubber Chemistry and Technology, **37**, 563–570 (1964).
https://doi.org/10.5254/1.3540348

[24] Hernández M., López-Manchado M. A., Sanz A., Nogales A., Ezquerra T. A.: Effects of strain-induced crystallization on the segmental dynamics of vulcanized natural rubber. Macromolecules, **44**, 6574–6580 (2011).
https://doi.org/10.1021/ma201021q

[25] Yeddes W., Diebali K., Wannes W. A., Horchani-Naifer K., Hammami M., Younes I., Tounsi M. S.: Gelatin-chitosan-pectin films incorporated with rosemary essential oil: Optimized formulation using mixture design and response surface methodology. International Journal of Biological Macromolecules, **154**, 92–103 (2020). https://doi.org/10.1016/j.ijbiomac.2020.03.092

[26] Jansen R. J. J., van Bekkum H.: XPS of nitrogen-containing functional groups on activated carbon. Carbon, **33**, 1021–1027 (1955). https://doi.org/10.1016/0008-6223(95)00030-H

[27] Ederer J., Janoš P., Ecorchard P., Tolasz J., Štengl V., Beneš H., Perchacz M., Pop-Georgievski O.: Determination of amino groups on functionalized graphene oxide for polyurethane nanomaterials: XPS quantitation *vs.* functional speciation. Royal Society of Chemistry, **7**, 12464–12473 (2017). https://doi.org/10.1039/C6RA28745J

[28] Bevas C. J., Abel M-L., Jacobs I., Watts J. F.: An interfacial chemistry study of methylene diphenyl diisocyanate and tantalum for heat exchanger applications. Surface and Interface Analysis, **52**, 685–693 (2020). https://doi.org/10.1002/sia.6845

[29] DeSanctis M. L., Soranno E. A., Messner E., Wang Z., Turner E. M., Falco R., Appiah-Madson H. J., Distel D. L.: Greater than pH 8: The pH dependence of EDTA as a preservative of high molecular weight DNA in biological samples. PLOS ONE, **18**, e0280807 (2023). https://doi.org/10.1371/journal.pone.0280807

[30] Barton A. F. M.: CRC handbook of solubility parameters and other cohesion parameters. CRC Press, Boca Raton (1991).

[31] Wang F., Wan L., Xu Z.: Graft polymerization of 2-hydroxyethyl methacrylate *via* ATRP with poly(acrylonitrile-*co*-*p*-chloromethyl styrene) as a macroinitiator. Science China Chemistry, **55**, 1125–1133 (2012). https://doi.org/10.1007/s11426-011-4462-0

[32] Tosaka M., Murakami S., Poompradub S., Kohjiya S., Ikeda Y., Toki S., Sics I., Hsiao B. S.: Orientation and crystallization of natural rubber network as revealed by WAXD using synchrotron radiation. Macromolecules, **37**, 3299–3309 (2004). https://doi.org/10.1021/ma0355608

[33] Schrieber R., Gareis H.: Gelatine handbook, theory and industrial practice. Wiley, Weinheim (2007).

[34] Gong Y., Xu X., Aquib M., Zhang Y., Yang W., Chang Y., Peng H., Boyer C., Whittaker A. K., Fu C.: Ammonium, phosphonium, and sulfonium polymers for antimicrobial applications: A comparative study. ACS Applied Polymer Materials, **6**, 6966–6975 (2024). https://doi.org/10.1021/acsapm.4c00461

[35] Jiao Y., Niu L-N., Ma S., Li J., Tay F. R., Chen J-H.: Quaternary ammonium-based biomedical materials: State-of-the-art, toxicological aspects and antimicrobial resistance. Progress in Polymer Science, **71**, 53–90 (2017). https://doi.org/10.1016/j.progpolymsci.2017.03.001

[36] Zhou Z., Zhou S., Zhang X., Zeng S., Xu Y., Nie W., Zhou Y., Xu T., Chen P.: Quaternary ammonium salts: Insights into synthesis and new directions in antibacterial applications. Bioconjugate Chemistry, **34**, 302–325 (2023). https://doi.org/10.1021/acs.bioconjchem.2c00598

[37] Painter P., Coleman M.: Essentials of polymer science and engineering. DEStech Publications, Pennsylvania (2009).

[38] Bunsanong A., Thongnuanchan B., Ninjan R., Salaeh S., Lopattananon N., Masa A.: Accelerator and zinc-free prevulcanized latex based on natural rubber-bearing benzyl chloride groups. Express Polymer Letters, **18**, 229–242 (2024). https://doi.org/10.3144/expresspolymlett.2024.16

[39] Tongnuanchan P., Benjakul S., Prodpran T.: Structural, morphological and thermal behaviour characterisations of fish gelatin film incorporated with basil and citronella essential oils as affected by surfactants. Food Hydrocolloids, **41**, 33–43 (2014). https://doi.org/10.1016/j.foodhyd.2014.03.015

[40] Fornaro T., Burini D., Biczysko M., Barone V.: Hydrogen-bonding effects on infrared spectra from anharmonic computations: Uracil-water complexes and uracil dimers. The Journal of Physical Chemistry A, **119**, 4224–4236 (2015). https://doi.org/10.1021/acs.jpca.5b01561

[41] Tongnuanchan P., Benjakul S., Prodpran T., Pisuchpen S., Osako K.: Mechanical, thermal and heat sealing properties of fish skin gelatin film containing palm oil and basil essential oil with different surfactants. Food Hydrocolloids, **56**, 93–107 (2016). https://doi.org/10.1016/j.foodhyd.2015.12.005